Quantitative study of the enhancement of bulk nonlinearities in metamaterials

Alec Rose, Stéphane Larouche, and David R. Smith
Center for Metamaterials and Integrated Plasmonics, Duke University, Durham, North Carolina 27708, USA
(Received 12 August 2011; published 2 November 2011)

Artificially structured metamaterials offer a means to enhance the weak optical nonlinearities of natural materials. The enhancement results from the inhomogeneous nature of the metamaterial unit cell, over which the local field distribution can likewise be strongly inhomogeneous, with highly localized and concentrated field regions. We investigate the nonlinear enhancement effect in metamaterials through a numerical study of four nonlinear metamaterial designs comprising arrays of metallic structures embedded in nonlinear dielectrics and operating around 10 THz. Through full-wave simulations and by employing an extended version of the transfer-matrix-based nonlinear parameter retrieval method, we confirm and quantify the enhanced nonlinearities, showing bulk quadratic nonlinear properties that are up to two orders of magnitude larger, and cubic nonlinear properties that are up to four orders of magnitude larger than the bulk nonlinear dielectric alone. Furthermore, the proposed nonlinear metamaterials support a variety of configurable nonlinear properties and regimes, including electric, magnetic, broadband, and low loss, depending on the particular geometry chosen. Finally, we use the retrieved parameters in a coupled-mode theory to predict the optimal crystal lengths and conversion efficiencies of these structures, displaying the possibility of efficient and subwavelength nonlinear devices based on metamaterials.

DOI: 10.1103/PhysRevA.84.053805 PACS number(s): 42.70.Mp, 42.65.Ky, 78.67.Pt

I. INTRODUCTION

Metamaterials, artificially structured mediums, engineered on the subwavelength scale from arrays of polarizable elements, have the potential to support nearly complete control over the entire set of macroscopic electromagnetic properties [1]. This flexibility, inherent to metamaterials, has been exploited to develop unusual and unprecedented optical media and devices, such as negative-index materials [2,3] and "invisibility cloaks" [4]. These media are formed by varying the linear effective constitutive parameters of the metamaterial throughout space, such that the propagation of waves through the medium is strongly and uniquely modified.

Nonlinear metamaterials (NLMMs) extend the range of opportunities for artificial electromagnetic materials, supporting nearly independent control of both the linear and nonlinear properties of the effective medium. Moreover, it was predicted early on that NLMMs could provide an avenue not just for adopting the nonlinearities of their constituent materials but also for enhancing them by orders of magnitude [5,6]. Fast-growing research in NLMMs has given glimpses of their potential in nonlinear optics, including demonstrations of frequency generation [7–10], parametric amplification [11,12], self-phase modulation and bistability [13–16], and several unique nonlinear processes with no analog in natural materials [17]. Alongside this research, a set of fundamental tools and techniques, similar to those that have been applied to the precise design of linear metamaterials, have been developed for NLMMs [18–20].

Enhancing the otherwise weak optical nonlinearities associated with natural materials is one of the most enticing capabilities of NLMMs. Metamaterials naturally support highly inhomogeneous field distributions, where electromagnetic energy can be concentrated into small, critical volumes [5]. Any nonlinear element placed in these volumes experiences a local field strength much greater than the average field. Enhancement of nonlinearities through light localization is well known and has been exploited in plasmonic media [21–25], photonic crystals [26,27], and resonant cavities [28,29]. However, there is a fundamental difference between the field localization in these structures and that associated with NLMMs: cavities and electromagnetic "hot spots" localize fields to tiny spatial volumes, restricting configurations to surfaces or similarly small fractions of the whole medium. Wave behavior in such systems is typically described in terms of scattering rather than propagation since the density and distribution of the enhancement regions are so sparse. In contrast, the field localization in NLMMs is distributed periodically throughout a volume with no fundamental constraint on wave propagation; in other words, the enhancement associated with NLMMs is inherently a bulk effect, imbuing the metamaterial composite with an effective, continuous nonlinear susceptibility many times greater than that of any of the constituent materials. This important distinction renders NLMMs an approach to the design of a new generation of materials with the potential for unprecedented bulk nonlinearities. Indeed, once designed, artificial materials of this type can subsequently be used in many of these same advantageous setups that are currently employed for natural materials, allowing for cumulative mechanisms of enhancement.

The basic analytic and experimental characterization of NLMMs has been achieved at microwave frequencies [18,30], where the nonlinearities are derived from packaged components, such as varactor diodes, integrated into metamaterial circuits. For these effective media, excellent agreement for both the linear and the nonlinear properties has been demonstrated between the designed and measured media. However, in designing NLMMs in the terahertz (THz) to visible wavelength range, it is far more reasonable to achieve the nonlinear properties through the inclusion of natural nonlinear materials. While the same theoretical and experimental approaches used in the design and characterization of microwave NLMMs can be applied to NLMMs composed of natural nonlinear materials, the magnitude of the enhancement has yet to be rigorously determined in these systems.

In this paper, we provide a quantitative, numerical analysis of the bulk nonlinear properties of four common metamaterial designs, each embedded in a generic nonlinear dielectric and operating around 10 THz. To begin with, we describe our method of analysis, namely, the transfer-matrix-based nonlinear retrieval method [19,20], and extend it to include both electric and magnetic nonlinearities. Next, we present the results of full-wave simulations of second-harmonic generation (SHG) and self-phase modulation (SPM) in each of the four proposed NLMMs, where SHG and SPM are intended to be representative of general second- and third-order nonlinear processes, respectively. Employing the extended nonlinear retrieval method, we use the resulting simulated spectrums to calculate the effective quadratic and cubic susceptibilities. The predicted enhancements are confirmed in the resonant structures, with values of up to two orders of magnitude in the quadratic processes and up to four orders of magnitude in the cubic processes. In addition, broadband enhancements of more than one and two orders of magnitude are demonstrated in the nonresonant structures. Next, using the retrieved parameters and coupled-mode theory, the optimal crystal lengths and maximum efficiencies of the NLMMs are calculated. Finally, we discuss the benefits, limitations, and fabrication feasibility of the proposed NLMMs, including the potential impact of NLMMs on the efficiency and compactness of nonlinear devices. The Appendix shows the derivation of the second-harmonic generation in a medium with a nonlinear response in both its electric polarization and magnetization.

II. THE NONLINEAR RETRIEVAL METHOD FOR MEDIA WITH NONLINEAR POLARIZATION AND MAGNETIZATION

The enhancement of nonlinear properties in NLMMs relates directly to the magnitude of the local field enhancement within the metamaterial elements. Full-wave simulations can offer direct measurements of the field-enhancement factor by simulating the excitation of either metamaterial or plasmonic structures; however, the results are specific to the setup employed and do not constitute a general description of an effective medium comprising such structures. The "enhancement factors" quoted in such studies are, at best, indirect measures of the resulting nonlinear properties [21,22,25]. Since it is our goal to demonstrate the enhancement of nonlinear optical processes in a bulk NLMM medium, we require a tool for the accurate computation of the NLMM's effective nonlinear properties, using the results of nonlinear scattering simulations on a single unit cell.

Previously, a method for the retrieval of the effective nonlinear susceptibilities from an inhomogeneous, nonlinear unit cell was introduced [19]. This technique, based on the nonlinear transfer-matrix method [31], takes as input the fields scattered by a layer of NLMM, returning the nonlinear susceptibility that exactly replicates the scattered fields of an equivalent, homogeneous nonlinear slab. The nonlinear retrieval method was extended to arbitrary three- and four-wave mixing processes [20] and successfully applied to several experiments [17,30], highlighting the applicability of the method in characterizing NLMMs.

To apply the nonlinear retrieval method for the structures studied here, however, some modifications are required. The retrieval method, as first introduced, is constrained by the assumption that only a nonlinear electric polarization or magnetization, but not both simultaneously, is present. This assumption fails explicitly for many mixed media NLMMs, such as the magnetic split-ring resonator embedded in a nonlinear dielectric. Furthermore, even for unit cells containing polarizable elements of only one type, a single nonlinear polarizability can still fail to characterize the structure in the presence of significant spatial dispersion [32]. In order to completely characterize a generic nonlinear medium, nonlinear dependences on the incident fields in the material's electric polarization *and* magnetization must be taken into account. In this section, a brief extension to the nonlinear retrieval method is outlined, allowing for the simultaneous retrieval of the nonlinear magnetic and electric susceptibilities contributing to any given wave-mixing process. For the full details of the existing nonlinear retrieval method, the reader is referred to [19,20].

It is well known that, for sufficiently weak excitations, the higher-order terms in the power-series expansion of a medium's polarization,

$$P = \epsilon_0 \left(\chi_e^{(1)} E + \chi_e^{(2)} E^2 + \chi_e^{(3)} E^3 + \cdots \right), \tag{1}$$

can be modeled simply as a radiating source, and likewise for the magnetization,

$$M = \chi_m^{(1)} H + \chi_m^{(2)} H^2 + \chi_m^{(3)} H^3 + \cdots, \tag{2}$$

invoking what is known as the first Born approximation [33]. A medium with a nonlinearity present in either its polarization or its magnetization can thus be modeled as having a distributed electric or magnetic source, respectively, whose magnitude and phase depend on the distribution of the exciting, or "fundamental," fields along with the corresponding higher-order susceptibility. For convenience, we will consider explicitly the electric fields scattered by an electric nonlinearity (denoted by subscript e) and the magnetic fields scattered by a magnetic nonlinearity (denoted by subscript m). Furthermore, because we are assuming weak excitations and neglecting cascaded interactions, it follows that we can neglect coupling between the electric and magnetic nonlinearities; i.e., the scattering associated with each nonlinearity is assumed to have no effect on the other.

As an example, we consider a one-dimensional three-layer structure in which an arbitrary nonlinear slab is sandwiched between semi-infinite regions of vacuum, as shown in Fig. 1(b). Under excitation by a set of linearly polarized monochromatic plane waves (the fundamental fields) and in the first Born approximation, the medium's nonlinear polarization and magnetization will produce radiating fields in the output and input vacuum regions. Assuming knowledge of the linear properties at the fundamental frequencies, the distribution of the fundamental fields can be completely solved for by transfer matrices. As such, the solution for the fundamental fields is omitted here, and the rest of the analysis will only involve the nonlinear scattered fields. We assume that the nonlinear slab, at the scattered frequency of interest, can be completely characterized by permittivity ϵ_2, permeability μ_2, and α-order

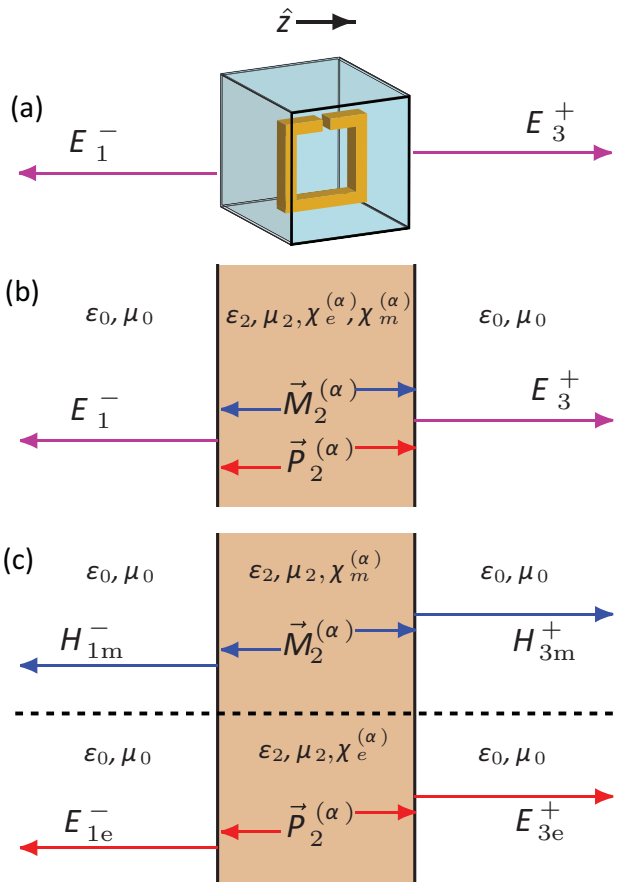

FIG. 1. (Color online) Sketch of the nonlinear retrieval process for metamaterials with simultaneous higher-order electric and magnetic susceptibilities. (a) The nonlinear scattering from an inhomogeneous unit cell, measured from simulation or experiment. (b) The equivalent three-layer system composed of a homogenized nonlinear slab sandwiched between regions of vacuum. (c) The magnetic (top) and electric (bottom) subproblems.

electric and magnetic nonlinear susceptibilities $\chi_e^{(\alpha)}$ and $\chi_m^{(\alpha)}$. In keeping with the notation of the existing nonlinear retrieval method, we split the fields into their forward (+) and backward (−) propagating parts, keeping track of the complex field amplitudes at the medium interfaces. Thus, the transmitted electric field, produced by a nonlinear electric polarization and located in the output medium at its interface with the nonlinear slab, is denoted by E_{3e}^{+}, while the reflected electric field, located in the input medium at its interface with the nonlinear slab, is denoted by E_{1e}^{-}. Similarly, the nonlinear magnetization generates H_{3m}^{+} and H_{1m}^{-}. If the nonlinear slab's higher-order susceptibilities are known, these fields can be analytically calculated according to the nonlinear transfer-matrix method. If, alternatively, the nonlinear susceptibilities involved are unknown and instead the scattered fields have been measured, as in the typical homogenization problem, the existing nonlinear retrieval method can be used to determine the effective nonlinearity *if only one nonlinearity is non-negligible*. If nonlinearities in both the magnetization and polarization simultaneously contribute to the scattered fields, then the problem must be reduced to a superposition of two independent homogenization problems: one considering only an electric nonlinearity with the associated scattered fields E_{3e}^{+} and E_{1e}^{-} and one considering only a magnetic nonlinearity with the scattered fields H_{3m}^{+} and H_{1m}^{-}. Once the subproblems have been properly defined, as in Fig. 1(c), the retrieval operation can be performed in each case, yielding effective values for both the electric and magnetic higher-order susceptibilities.

Obviously, we cannot probe the field contributions from the electric and magnetic nonlinearities individually since it is the *total* scattered fields, E_3^{+} and E_1^{-}, given by

$$E_3^{+} = E_{3e}^{+} + Z_0 H_{3m}^{+}, \tag{3}$$

$$E_1^{-} = E_{1e}^{-} - Z_0 H_{1m}^{-}, \tag{4}$$

that will be measured in any experiment or simulation, as in Fig. 1(a). Thus, our goal is to isolate the fields according to the nonlinear source that produced them (electric or magnetic) so that we can run each set of scattered fields through an independent retrieval procedure. In the transfer-matrix retrieval method the field-to-susceptibility ratios $E_{3e}^{+}/\chi_e^{(\alpha)}$ and $E_{1e}^{-}/\chi_e^{(\alpha)}$, and likewise for the magnetic terms, are needed. The method for calculation of these quantities is given elsewhere [20] and requires only the thickness of the sample and its effective linear properties as inputs. Taking the ratio of these two quantities, we can compute the ratios of the reflected to the transmitted scattered fields for each process, which we denote as

$$R_e = E_{1e}^{-}/E_{3e}^{+}, \tag{5}$$

$$R_m = H_{1m}^{-}/H_{3m}^{+}. \tag{6}$$

We reiterate that these ratios can be calculated analytically, employing slightly modified equations from the nonlinear transfer-matrix method and without any knowledge of the nonlinear susceptibility involved. We thus arrive at four equations and four unknowns, which can be rearranged to give

$$E_{3e}^{+} = \frac{R_m E_3^{+} + E_1^{-}}{R_e + R_m}, \tag{7}$$

$$H_{3m}^{+} = \frac{1}{Z_0}\frac{R_e E_3^{+} - E_1^{-}}{R_e + R_m}, \tag{8}$$

and similarly for the reflected fields. Finally, we are able to merge the above analysis with the preexisting nonlinear retrieval method, yielding the following retrieval equations:

$$\chi_e^{(\alpha)} = \frac{\frac{R_m E_3^{+} + E_1^{-}}{R_e + R_m}}{E_{3e}^{+}/\chi_e^{(\alpha)}}, \tag{9}$$

$$\chi_m^{(\alpha)} = \frac{\frac{1}{Z_0}\frac{R_e E_3^{+} - E_1^{-}}{R_e + R_m}}{H_{3m}^{+}/\chi_m^{(\alpha)}}. \tag{10}$$

These represent slight modifications to the former nonlinear retrieval equations. In contrast to the previous method, these equations make use of both the transmitted and reflected spectrums but still require measurements from only a single experiment or simulation. However, Eqs. (9) and (10) now retrieve both electric and magnetic contributions in a given nonlinear process, allowing for the complete characterization of more general NLMMs. While the presence of both electric and magnetic nonlinear susceptibilities is rare for naturally

occurring materials, the situation is very common for NLMMs, thus motivating the modifications considered here.

The modified retrieval procedure described above is sufficient to analyze the structures in the following sections. We note, however, that we ignore any effects due to magnetoelectric coupling between unit cells either in the fundamental or the harmonics. The presence of magnetoelectric coupling causes an intercell interaction that cannot be accounted for in retrievals based on one unit cell of metamaterial. Because magnetoelectric coupling appears to be of concern only when both the electric and magnetic responses are simultaneously resonant, its neglect here is reasonable for the configurations we consider [32,34–36].

III. SIMULATIONS AND RETRIEVALS

In this section, we analyze the nonlinearity enhancement effect in the context of four distinct types of NLMM structures: the electric-field-coupled resonator (ELC), the split-ring resonator (SRR), the cut-wire medium, and the I-beam medium. The nonlinearity in each case comes from a generic nonlinear dielectric matrix in which the metallic structure is embedded. Full-wave, frequency-domain simulations, using the COMSOL multiphysics suite [37], are performed on a single unit cell of each NLMM, with the appropriate nonlinear equations evaluated in the dielectric matrix. Periodic boundary conditions are used to simulate a metamaterial slab with infinite extent in the transverse directions. The metal structures are assumed to be silver, which is modeled with a Drude dispersion using a plasma frequency of 2.179×10^{15} Hz and a relaxation rate of 4.352×10^{12} Hz [38]. The dielectric medium is modeled with a permittivity of $2.40\epsilon_0$. Two nonlinear processes, corresponding to two distinct NLMMs, are considered for each metamaterial: SHG in the case of embedding in a second-order nonlinear dielectric and SPM in the case of a third-order nonlinear, or Kerr, dielectric. The simulations consist of two distinct domains for the fundamental and nonlinear scattered fields. The fundamental fields are solved for first, neglecting the nonlinearity, consistent with the nondepleted pump approximation. The distribution of the fundamental fields is then used in the calculation of the nonlinear polarization in the dielectric, which operates as a distributed source in the second, nonlinear scattering domain. This two-part design strictly enforces the first Born approximation, prohibiting all cascaded and cyclic nonlinear effects. This is true even in the case of SPM, where, despite the degeneracy in frequency, the nonlinear scattered fields are kept separate from the fundamental fields. The validity and self-consistency of these simulations have been verified on simple, homogeneous slabs of nonlinear dielectric.

For each simulation, the unit cell is excited by a plane wave traveling in the positive z direction, with the electric field polarized along the x axis. The linear properties are retrieved using the standard scattering-parameter retrieval techniques [39–41], while the fields scattered by the presence of the appropriate nonlinearity are measured at the output and input ports and fed into the above nonlinear retrieval equations. For the simulations of SHG, the retrieval equations yield the effective electric and magnetic second-order susceptibilities $\chi^{(2)}_{e,xxx}(2\omega;\omega,\omega)$ and $\chi^{(2)}_{m,yyy}(2\omega;\omega,\omega)$, respectively. For SPM, the retrieved parameters are the effective electric and magnetic third-order susceptibilities $\chi^{(3)}_{e,xxxx}(\omega;\omega,-\omega,\omega)$ and $\chi^{(3)}_{m,yyyy}(\omega;\omega,-\omega,\omega)$, respectively. Though the local fields will inevitably contain multiple field components, the boundary conditions at the ports enforce the scattered waves to be the same polarization as the incident wave. Thus, even though the local fields will probe all elements of the local nonlinear tensor in the dielectric, the simulations will ultimately investigate just a single element of each of the NLMM's *effective* nonlinear tensors. The polarization and orientation used in the following simulations were chosen to ensure maximum coupling between the incident wave and the structure. Though it is not presented here, the full effective linear and nonlinear tensors can be retrieved by the same procedure, provided that the appropriate polarizations of the various contributing waves are enforced. In the following sections, the tensorial notation in the material properties is omitted for brevity.

The higher-order susceptibility alone, however, is not an adequate measure of the enhancement over the bulk embedding medium due to the simultaneous effect of the periodic inclusions on the medium's impedance. Instead, we define the material figure of merit (see the Appendix),

$$\kappa^{(2)} = \frac{Z(\omega)\sqrt{Z(2\omega)}}{Z_0}\chi_e^{(2)} + \frac{Z_0}{Z(\omega)\sqrt{Z(2\omega)}}\chi_m^{(2)}, \qquad (11)$$

where $Z(\omega) = \sqrt{\frac{\mu(\omega)}{\epsilon(\omega)}}$ is the effective impedance of the NLMM and Z_0 is the impedance of free space. This is a slight modification to the usual definition in a purely electric medium (see [42], p. 445). With this definition, the corresponding material figure of merit of the nonlinear dielectric alone is

$$\kappa_d^{(2)} = \frac{Z_d^{3/2}}{Z_0}\chi_d^{(2)}, \qquad (12)$$

where the subscript d refers to the properties of the dielectric. For consistency, we define an analogous material figure of merit for SPM,

$$\kappa^{(3)} = \frac{Z(\omega)^2}{Z_0}\chi_e^{(3)} + \frac{Z_0}{Z(\omega)^2}\chi_m^{(3)}, \qquad (13)$$

with units of m^2/W. It can be shown that the first-order correction in the power-dependent refractive index is directly related to this figure and given by $\Delta n = \frac{3}{4}\kappa^{(3)} I$, where I is the field intensity. The material figure of merit in the third-order nonlinear dielectric alone is given by

$$\kappa_d^{(3)} = \frac{Z_d^2}{Z_0}\chi_d^{(3)}. \qquad (14)$$

We reiterate here that the deviations of the NLMM's effective nonlinearities from that of the embedding medium are not due to the addition of nonlinearities, as we neglect the nonlinearity of the metal structures themselves, but rather, they come from the induced localization of the fundamental fields within the embedding dielectric. Additionally, since the retrieved properties are necessarily a sort of average over the whole unit cell, it may seem that the small volumes in which the majority of the field localization occurs will have the effect of counterbalancing the enhancement. Indeed, the additional

nonlinear activity in the areas of high field concentration will be accompanied by reduced nonlinear activity in the areas of low field concentration. However, since the local nonlinear effects scale as higher-order powers of the local fields, the field localization is in effect weighted more strongly than the effective reduction in contributing volume, and consequently, the bulk nonlinear susceptibility must take on a larger value than the background medium alone. To measure the degree of field localization, we introduce the localization factor, analogous to the enhancement factors employed in previous plasmonic studies [21,22],

$$L(|E|^{\alpha}) = \frac{\int_V |E_{\mathrm{MM}}(\vec{r})|^{\alpha} d\vec{r}^3}{\int_V |E_{\mathrm{hom}}(\vec{r})|^{\alpha} d\vec{r}^3}, \tag{15}$$

where the numerator is a volume integral of the fundamental electric-field norm raised to the α power, integrated over the metamaterial unit cell. The denominator is the same integral but for a homogeneous slab with equivalent linear properties. Thus, $L(|E|^{\alpha})$ is a direct measure of the degree of inhomogeneity in the fields within the metamaterial, normalized by an otherwise equivalent homogeneous medium. As we show in the following sections, the deviations of the NLMM's effective nonlinearities from that of the embedding medium can be quite dramatic, especially when the structures are operated near resonance, where the second- and third-order localization factors reach their maximums.

A. The nonlinear electric-field-coupled resonator

The ELC is a resonant metamaterial structure designed to exhibit an electric resonance [43]. The dominant coupling of the incident fields into and out of this structure is capacitive, and thus it is classified as an electric resonator. At resonance, the incident electric fields become highly confined in the capacitive gaps, as shown in Fig. 2(b), making this an ideal structure for the resonant enhancement of the nonlinearities of any medium placed in these gaps.

The ELC employed here, displayed in Fig. 2(a), is composed of 50-nm-thick, 100-nm-wide silver with two 100-nm gaps. The outer dimensions of the silver pattern are 1.6 μm, while the ELC itself is arranged in a cubic lattice with a lattice constant of 2 μm. For the SHG simulation, the nonlinear dielectric is given a nonzero second-order electric susceptibility for both fundamental and harmonic fields polarized in the x direction. All other elements of the nonlinear tensors, both second and third order, are zero. For SPM, the dielectric's nonlinearity takes the form of a nonzero third-order electric susceptibility for fields polarized in the x direction. The retrieved linear properties are shown in Fig. 2(c). The retrieved values of the second-order and third-order susceptibilities and material figures of merit, normalized by the nonlinear dielectric, are displayed in Figs. 2(e)–2(j). The higher-order magnetic susceptibilities are normalized by the impedance of free space where appropriate.

As expected, the retrieved nonlinearities of the ELC show massive enhancements near the ELC's resonance. The

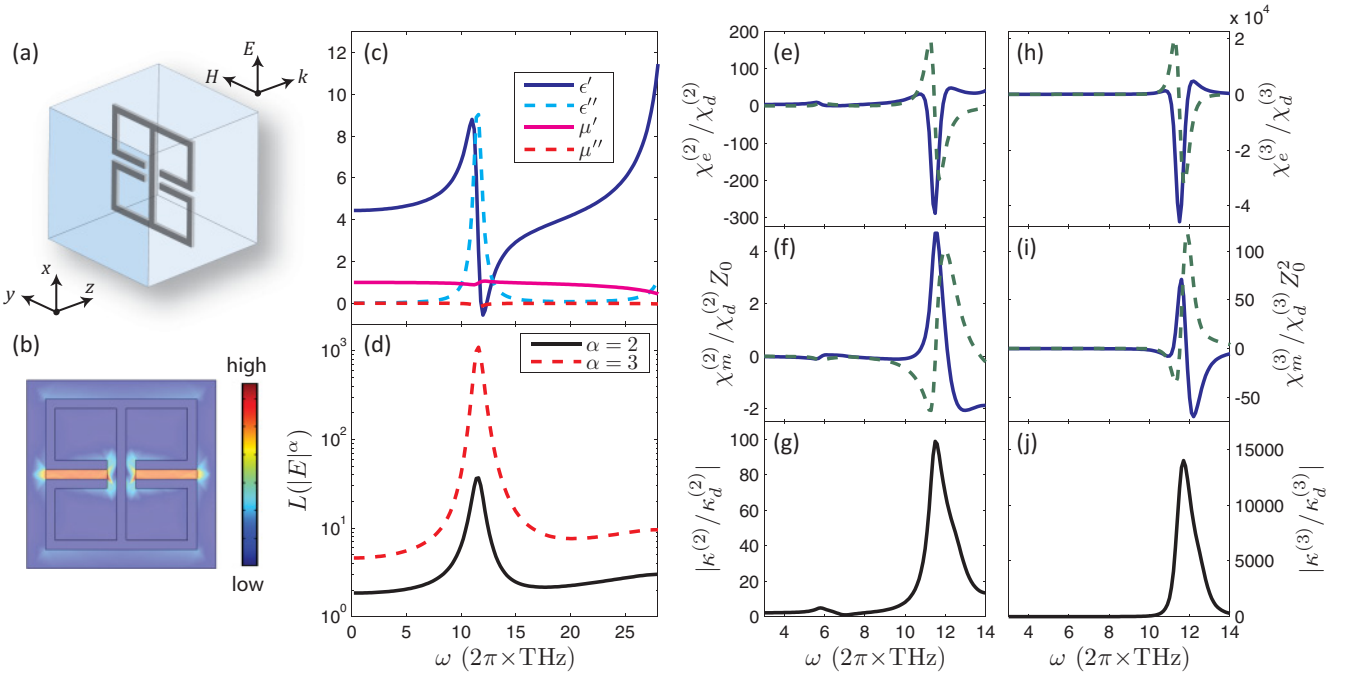

FIG. 2. (Color online) (a) An ELC embedded in a nonlinear dielectric. (b) The electric-field norm at the resonance frequency. (c) The retrieved linear properties. (d) Log-scale plot of the second- and third-order electric-field localization factors [Eq. (15)]. (e)–(j) The retrieved electric and magnetic higher-order susceptibilities and corresponding material figures of merit, normalized by the nonlinear bulk dielectric: (e)–(g) are the second-order properties corresponding to SHG, and (h)–(j) are the third-order properties corresponding to SPM. The real (solid blue curve) and imaginary (dashed green curve) parts are shown for the higher-order susceptibilities.

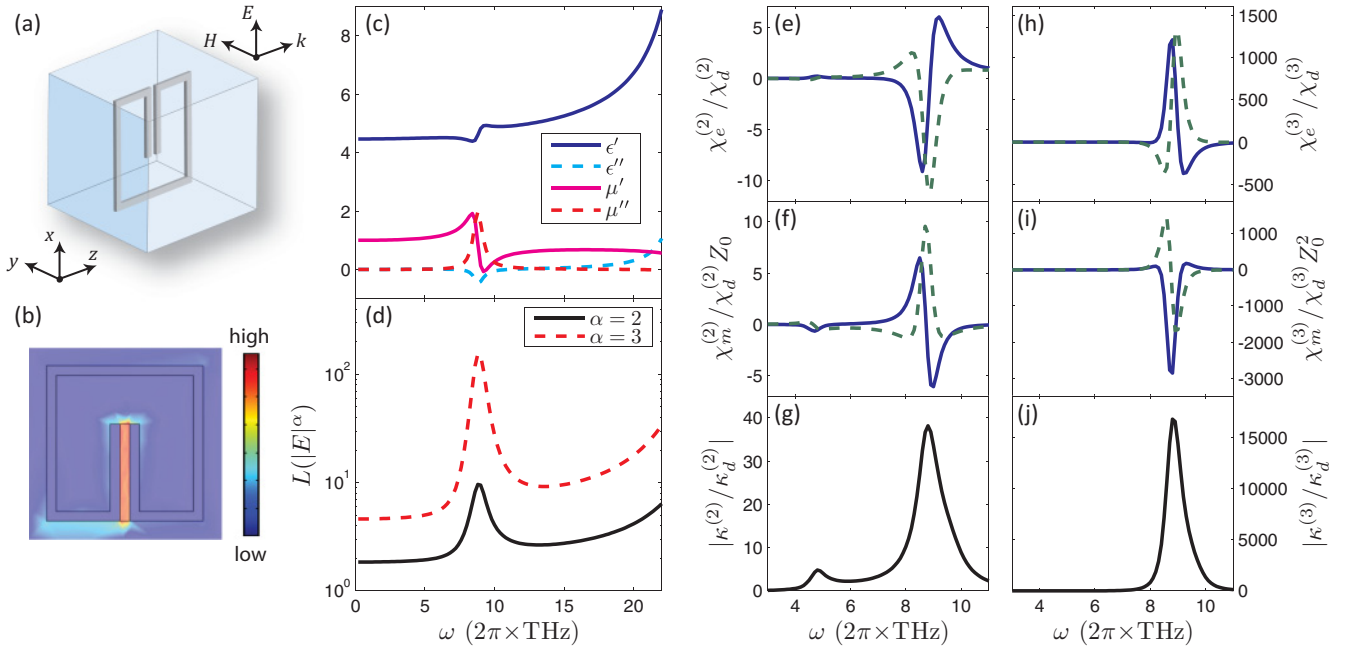

FIG. 3. (Color online) (a) An SRR embedded in a nonlinear dielectric. (b) The electric-field norm at the resonance frequency. (c) The retrieved linear properties. (d) Log-scale plot of the second- and third-order electric-field localization factors [Eq. (15)]. (e)–(j) The retrieved electric and magnetic higher-order susceptibilities and corresponding material figures of merit, normalized by the nonlinear bulk dielectric: (e)–(g) are the second-order properties corresponding to SHG, and (h)–(j) are the third-order properties corresponding to SPM. The real (solid blue curve) and imaginary (dashed green curve) parts are shown for the higher-order susceptibilities.

second-order and third-order figures of merit show peak values that are two orders and four orders of magnitude larger than the embedding nonlinear dielectric, respectively. The retrieved nonlinear susceptibilities themselves also show the expected Lorentzian features in their real and imaginary parts. It is noteworthy that the second-order properties show weaker (one order of magnitude) enhancements when the fundamental frequency corresponds to half the resonance frequency. This behavior has been predicted before in several analytical studies [18,33]. The nonlinear ELC also seems to support a non-negligible magnetic nonlinearity in both the SHG and SPM retrievals. However, the excitation of a magnetic moment in this structure for this particular polarization is impossible, and so these nonlinearities must be attributed to spatial dispersion. While spatial dispersion in the nonlinear properties of metamaterials will be treated elsewhere [44], we content ourselves here by noting that the magnetic properties have roughly a π phase relation with the corresponding electric properties, akin to the "antiresonance" features common to linear metamaterial retrievals [45].

B. The nonlinear split-ring resonator

The second structure we consider is the SRR, displayed in Fig. 3(a), which also exhibits an LC-type resonance. In contrast to the ELC, however, the dominant coupling in this structure is inductive, coming from magnetic flux passing through the interior of the metallic ring. As such, the SRR is a magnetic resonator, and on resonance the electric fields, shown in Fig. 3(b), become highly confined in the capacitive gap. Though the only nonlinearity present is the electric nonlinearity of the dielectric medium, the coupling of the generated electric fields to the magnetic resonance of the SRR makes the dominant effective nonlinearity magnetic in nature.

Like the ELC, the SRR is composed of 50-nm-thick, 100-nm-wide silver, but with a single 100-nm gap. The outer dimensions and lattice constant are identical to the ELC. However, since the capacitive gap is rotated compared to the ELC, the highly localized electric fields of the SRR are dominant in the z direction. Thus, the dielectric's nonlinearities considered in these simulations only involve fields polarized in the z direction, and, again, all other elements of the dielectric's nonlinear tensors are set to zero. The retrieved linear, second-order, and third-order properties are displayed in Figs. 3(c)–3(j).

Again, for excitation near the resonance frequency of the SRR, the retrieved nonlinearities are highly enhanced compared to the bulk nonlinear dielectric. Many of the same features in the retrieval of the ELC are present, but with the difference that the effective nonlinearities are mostly magnetic in nature. The spatial dispersion effects are also slightly mitigated due to the lower resonance frequency of the SRR. Furthermore, while the SPM material figure of merit is slightly larger for the SRR, the ELC shows roughly double the enhancement in SHG. This can be explained in terms of the necessary overlap of the field distributions at the fundamental and second-harmonic frequencies required for efficient conversion in a bulk material, similar to the nonlinear coupling between different modes in a waveguide. Because the x component of the local electric field is dominant at

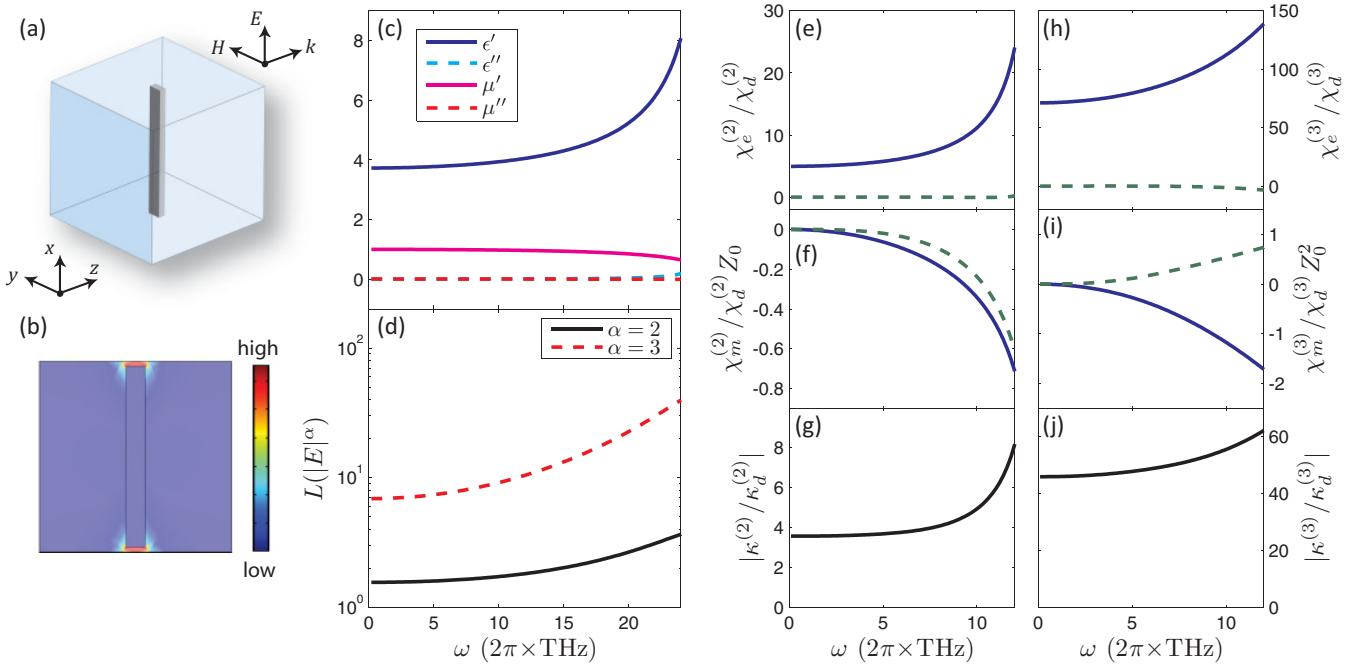

FIG. 4. (Color online) (a) A cut-wire medium embedded in a nonlinear dielectric. (b) The electric-field norm at 10 THz. (c) The retrieved linear properties. (d) Log-scale plot of the second- and third-order electric-field localization factors [Eq. (15)]. (e)–(j) The retrieved electric and magnetic higher-order susceptibilities and corresponding material figures of merit, normalized by the nonlinear bulk dielectric: (e)–(g) are the second-order properties corresponding to SHG, and (h)–(j) are the third-order properties corresponding to SPM. The real (solid blue curve) and imaginary (dashed green curve) parts are shown for the higher-order susceptibilities.

all frequencies in the ELC, the coupling between the field distributions at different frequencies is more efficient than in the SRR, where the z component of the local electric field is only strong for frequencies sufficiently close to the resonance. For SPM, where all involved frequencies are degenerate, the mode overlap is identically unity in both structures.

C. The nonlinear cut-wire medium

The cut-wire medium, on the other hand, can be employed as a nonresonant metamaterial, often to provide a relatively broadband electric response. Though this medium will lack the dramatic resonance-induced enhancements of the SRR and ELC, it supports an inhomogeneous field distribution, as seen in Fig. 4(b), with electric fields weakly confined to the capacitive gap between neighboring cut wires. Like the ELC, coupling between this structure and the incident fields is capacitive in nature.

The cut-wire structure, shown in Fig. 4(a), is composed of a silver rectangular rod, 100 nm thick and 200 nm wide, with a gap of 100 nm between neighboring cut wires. These dimensions are thicker than the previous structures in order to reduce the cut wire's effective inductance, ensuring operation well below the structure's resonance. The lattice constant is 2 μm in all directions. For the SHG simulation, the embedding dielectric is given a nonzero second-order electric susceptibility for both fundamental and harmonic fields polarized in the x direction. For SPM, the dielectric's nonlinearity takes the form of a nonzero third-order electric susceptibility for fields polarized in the x direction. The retrieved linear, second-order, and third-order properties are displayed in Figs. 4(c)–4(j).

The retrieved nonlinearities of the cut-wire medium are very different from the previous two resonant structures. For a fundamental frequency of 10 THz, roughly the frequency of interest for this analysis, the enhancement in SHG is fivefold, while the nonlinearity for SPM is 56 times greater than the nonlinear dielectric alone. While these enhancements are much less dramatic than the resonant SRR and ELC, they deserve some discussion. Unlike its resonant counterparts, the cut-wire medium shows fairly broadband enhancements of the material figures of merit, asymptoting at low frequencies to values greater than unity. Moreover, these enhancements are not accompanied by significant losses. In fact, the effective loss tangents at 10 and 20 THz in the cut-wire medium are just 1.1×10^{-3} and 2.8×10^{-3}, respectively. Spatial dispersion effects are also much less prominent. Thus, there exists a significant trade-off between resonant and nonresonant metamaterial structures in terms of enhancing nonlinear phenomena.

D. The nonlinear I-beam structure

The I-beam structure belongs to the same category of nonresonant electric metamaterials as the previous cut-wire medium, but with the extended arms providing additional capacitance. Due to the increased capacitance, the I beam supports a stronger electric response and confines a greater fraction of the incident field to the gaps between neighboring

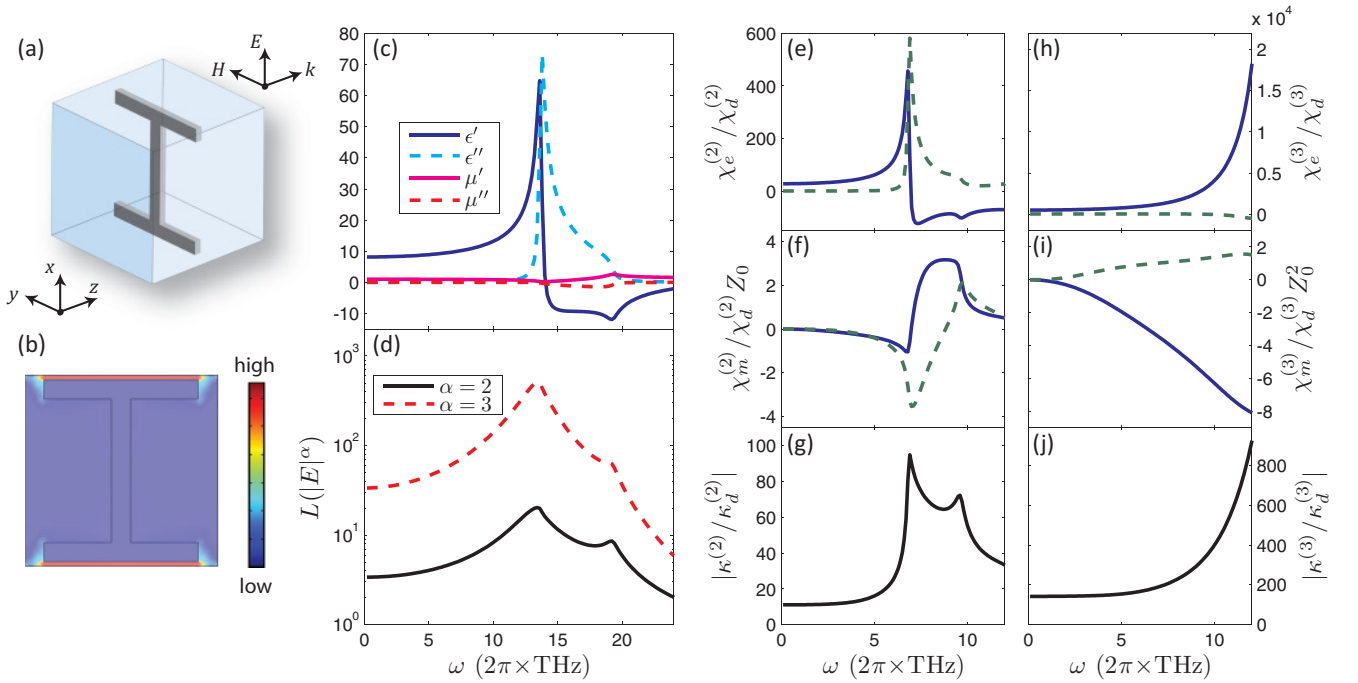

FIG. 5. (Color online) (a) An I-beam structure embedded in a nonlinear dielectric. (b) The electric-field norm at 10 THz. (c) The retrieved linear properties. (d) Log-scale plot of the second- and third-order electric-field localization factors [Eq. (15)]. (e)–(j) The retrieved electric and magnetic higher-order susceptibilities and corresponding material figures of merit, normalized by the nonlinear bulk dielectric: (e)–(g) are the second-order properties corresponding to SHG, and (h)–(j) are the third-order properties corresponding to SPM. The real (solid blue curve) and imaginary (dashed green curve) parts are shown for the higher-order susceptibilities.

structures than the cut-wire medium, as seen in Figs. 5(b) and 5(d). Thus, this medium can be expected to show a strong, broadband enhancement of the embedding medium's nonlinearities.

The I beam, displayed in Fig. 5(a), consists of 100-nm-thick, 200-nm-wide silver in the shape of an I, with arms that extend 1.6 μm from tip to tip. The lattice constant and gap between neighboring I beams are 2 μm and 100 nm, respectively. The embedding dielectric used is the same as the nonlinear cut-wire and ELC mediums. The retrieved linear, second-order, and third-order properties are displayed in Figs. 5(c)–5(j).

As expected, the I-beam structure shows similar features to the cut-wire medium, but with much larger overall enhancements. For a fundamental frequency of 10 THz, the SHG and SPM material figures of merit are enhanced by a factor of 55 and 400, respectively, both roughly an order of magnitude larger than the cut-wire medium. However, the usable frequency range of the I-beam structure is significantly reduced: the capacitance is so large that the resonance frequency of this structure is brought into view. The massive spatial dispersion in both the linear and nonlinear properties call into question the validity of the SHG retrieval at 10 THz, as the second-harmonic frequency passes through the resonance frequency well below the 10-THz target frequency for the fundamental. However, the low-frequency asymptotic value for SHG is still valid along with the SPM results, which do not suffer from involving a frequency at twice the fundamental frequency. Additionally, at 10 THz, the effective loss tangent is 1.1×10^{-2}, more than small enough to consider the nearly three orders of magnitude enhancement in the SPM material figure of merit a low-loss, nonresonant effect. Thus, there exists a trade-off between the cut-wire and I-beam structures, where the operational frequencies, the loss tangent, and the magnitude of the enhancement can be weighed against one another for a given application.

IV. CALCULATION OF THE NONLINEAR CONVERSION EFFICIENCIES

The retrieved parameters of the previous section fully characterize the four nonlinear metamaterials, allowing for the metamaterials to be analyzed as if they were perfectly homogeneous materials. Thus, we are in a position to give a more thorough analysis of the NLMMs in terms of their applicability in realistic nonlinear devices. In particular, the NLMMs presented here offer competing effects in the enhancement of nonlinear phenomena: on the one hand, they show nonlinearities that are orders of magnitude larger than the embedding medium alone; on the other hand, the periodic metallic inclusions are a major source of ohmic losses, constraining the maximum lengths of any resulting devices. Before NLMMs can be endorsed as an avenue to improving on existing nonlinear devices, the NLMM enhancement effect must be weighed against the accompanying losses in the context of realistic device specifications. In this section, using a coupled-mode theory derived for homogeneous materials, we calculate the figures of merit and conversion efficiencies for nonlinear devices based on slabs of the four NLMMs, analyzing both the second- and third-order processes. We

show that, despite the severe constraints imposed by material losses, the NLMMs are able to support reasonable conversion efficiencies in the form of compact, even subwavelength, devices.

A. Second-harmonic generation

SHG from a monochromatic, planar wave, traveling in a homogeneous second-order nonlinear medium, can be described by a coupled-mode analysis. Using the simplifying assumptions of nondepleted pump and slowly varying amplitude, the following expression can be derived for the output second-harmonic intensity [42]:

$$I_{\text{out}}(2\omega) = \frac{\omega^2}{2c^2}|\kappa^{(2)}|^2[I_{\text{in}}(\omega)]^2 L^2 h(L), \tag{16}$$

where L is the total interaction length, $I_{\text{in}}(\omega)$ is the input intensity of the fundamental wave, and

$$h(L) = \exp\left[-\left(\frac{\alpha(2\omega)}{2} + \alpha(\omega)\right)L\right]\frac{[\sinh(\Delta\alpha L/2)]^2}{(\Delta\alpha L/2)^2} \tag{17}$$

contains the contributions from the absorption coefficients $\alpha(\omega)$ at both frequencies, where $\Delta\alpha$ is given by

$$\Delta\alpha = \frac{\alpha(2\omega)}{2} - \alpha(\omega). \tag{18}$$

Note that, for the sake of narrowing the focus of the analysis, the terms dependent on the phase mismatch between the interacting waves have been removed.

From the above, we can define the system's conversion efficiency as

$$\eta^{(2)} = \frac{I_{\text{out}}(2\omega)}{I_{\text{in}}(\omega)} = \frac{\omega^2}{2c^2}|\kappa^{(2)}|^2 L^2 h(L) I_{\text{in}}(\omega). \tag{19}$$

In determining the maximum efficiency and the corresponding device length for SHG, we find the quantity $L^2h(L)$ to be maximized by an optimum interaction length

$$L_{\text{opt}} = \frac{2}{\Delta\alpha}\tanh^{-1}\left(\frac{\Delta\alpha}{\alpha(2\omega)/2 + \alpha(\omega)}\right). \tag{20}$$

For interaction lengths longer than L_{opt}, linear absorption begins to dominate, and the conversion efficiency declines.

We use Eqs. (19) and (20), together with the retrieved parameters of the four NLMMs, to calculate realistic device sizes and efficiencies. For the ELC and SRR, we choose optimum fundamental frequencies close to the respective resonance frequencies to maximize the resonant enhancement. A fundamental frequency of 10 THz is used for the cut-wire medium, while the I-beam structure, to avoid significant spatial dispersion, is operated at 5 THz, noting that the efficiencies of these nonresonant structures are characteristic of broad frequency bands. The ratio of the efficiencies of the NLMMs to the nonlinear dielectric alone is given by

$$F(\eta^{(2)}) = \frac{\eta^{(2)}}{\eta_d^{(2)}} = h(L)\left|\frac{\kappa^{(2)}}{\kappa_d^{(2)}}\right|^2. \tag{21}$$

This quantity directly compares devices of the same lengths, operating frequencies, and input powers, while taking into account both the enhancement effect and the additional losses introduced by the periodic metallic inclusions. Thus, $F(\eta^{(2)})$ represents a complete, albeit simplistic, measure of the relative performances of NLMMs and natural materials as frequency doublers. The optimum lengths and efficiencies for all four NLMMs are displayed in Table I, assuming a value of $\chi_d^{(2)} = 20$ pm/V for the embedding nonlinear dielectric and an input intensity of $I_{\text{in}}(\omega) = 40$ MW/cm^2.

TABLE I. Optimal lengths, efficiencies, and normalized efficiencies for SHG in each NLMM. The conversion efficiencies are calculated using the value $\chi_d^{(2)} = 20$ pm/V for the nonlinear dielectric and assuming an input intensity of 40 MW/cm^2.

NLMM	ω ($2\pi\times$THz)	L_{opt} (μm)	$\eta^{(2)}/10^{-6}$	$F(\eta^{(2)})$
ELC	11.4	4	8.65	1170
SRR	8.6	4	1.07	253
Cut wire	10	650	456.12	3.03
I beam	5	216	132.32	31.9

Though the above analysis ignores the role of phase matching, this interesting and crucial factor deserves a few words. In principal, conventional approaches to phase matching [33] should be largely applicable to NLMMs based on periodic inclusions in a nonlinear dielectric by applying the same techniques to the embedding medium itself. However, due to the range and configurability in their linear properties, NLMMs may offer unique advantages in overcoming phase mismatch. For example, a number of recent studies have revealed unique configurations for phase matching and quasiphase matching (QPM) that are singular to NLMMs [11,17,46,47]. Furthermore, the relatively small interaction lengths proposed in Table I have the added effect of relaxing the constraints imposed by phase mismatch. As a numerical example, the coherence length in the nonlinear ELC for a fundamental frequency of 11.4 THz is $L_{\text{coh}} = 2\pi/\Delta k = 14.9$ μm, which is actually *larger* than the optimum interaction length, making phase mismatch essentially a nonfactor in this structure. Thus, phase matching should not pose a significant challenge to the implementation of NLMMs in nonlinear devices and could ultimately prove to be an advantage. A detailed analysis of phase matching in NLMMs will be treated in a subsequent study [48].

B. Self-phase modulation

Among third-order nonlinear processes, SPM has unique applications with its own set of definitions and figures of merit. However, since it is our intention to investigate the enhancement properties of NLMMs on third-order processes in general, we omit a discussion of the particulars of SPM and instead describe the process through a coupled-mode analysis, analogous to SHG. Specifically, we continue to invoke the nondepleted pump approximation and calculate the intensity of the nonlinear scattered fields. Though the nondepleted pump is inappropriate for describing most devices involving SPM, such as directional couplers, the following analysis and figures of merit have the advantage of being readily applicable to third-order processes in general, such as nondegenerate four-wave mixing. For a more detailed analysis

TABLE II. Optimal lengths and conversion efficiencies for SPM in each NLMM. The conversion rates are calculated using the value $\chi_d^{(3)} = 10^{-20}$ m^2/V^2 for the nonlinear dielectric.

NLMM	ω ($2\pi\times$THz)	L_{opt} (μm)	$\eta^{(3)}/10^{-7}$	$F(\eta^{(3)})$
ELC	11.5	2	4.25	8.25×10^6
SRR	8.7	2	8.70	2.95×10^7
Cut wire	10	1124	51.28	417
I beam	10	66	9.39	2.21×10^4

of metamaterials for optical switching and related applications, the reader is referred to Ref. [49].

Let us consider a monochromatic, planar wave traveling in a homogeneous third-order nonlinear medium. In the nondepleted pump limit and taking the slowly varying amplitude approximation, we can describe the SPM process in terms of the intensity of the nonlinear scattered fields, given by

$$I_{\text{out}}^{\text{NL}}(\omega) = \frac{9}{16}\frac{\omega^2}{c^2}|\kappa^{(3)}|^2 L^2 g(L)\left[I_{\text{in}}^{\text{FF}}(\omega)\right]^3, \tag{22}$$

where

$$g(L) = \exp\left[-2\alpha(\omega)L\right] \tag{23}$$

contains the effect of propagation losses on efficiency. It follows that the conversion efficiency is given by the ratio of the nonlinear scattered intensity to the input intensity,

$$\eta^{(3)} = \frac{I_{\text{out}}^{\text{NL}}(\omega)}{I_{\text{in}}^{\text{FF}}(\omega)} = \frac{9}{16}\frac{\omega^2}{c^2}|\kappa^{(3)}|^2 L^2 g(L)\left[I_{\text{in}}^{\text{FF}}(\omega)\right]^2. \tag{24}$$

As before, we find an optimum interaction length by maximizing the quantity $L^2 g(L)$, so that maximum efficiency is obtained for a slab of length

$$L_{\text{opt}} = \frac{1}{\alpha(\omega)}. \tag{25}$$

Normalizing Eq. (24) by the efficiency of the dielectric alone, we arrive at the figure of merit describing the enhancement of third-order nonlinear process in the four NLMMs:

$$F(\eta^{(3)}) = \frac{\eta^{(3)}}{\eta_d^{(3)}} = g(L)\left|\frac{\kappa^{(3)}}{\kappa_d^{(3)}}\right|^2. \tag{26}$$

The optimum lengths and conversion efficiencies for SPM in the four NLMMs are displayed in Table II, assuming a value of $\chi_d^{(3)} = 10^{-20}$ m^2/V^2 for the embedding nonlinear dielectric and an input intensity of $I_{\text{in}}(\omega) = 40$ MW/cm^2.

In the resonant structures for both the second-order and third-order nonlinear processes, however, the linear absorption in the metamaterials is strong enough to potentially invalidate the slowly varying amplitude approximation. In order to verify the above results, the conversion efficiencies of the ELC and SRR were calculated directly using the nonlinear transfer-matrix method [31], finding the error to be less than 25% in all cases.

V. DISCUSSION AND CONCLUSION

The resonant ELC and SRR structures showed the largest enhancements to the nonlinearities of the embedding medium, roughly two and four orders of magnitude for SHG and SPM, respectively. However, the resonant nature of these structures brings with it a narrow band of operation as well as extreme losses. Thus, applications utilizing these structures will likely be constrained to slabs only a handful of unit cells thick, as is demonstrated in Tables I and II. Still, the sheer magnitude of the enhancement makes these structures intriguing, allowing even subwavelength slabs to support reasonable conversion efficiencies. The cut-wire and I-beam structures, on the other hand, can operate in the nonresonant regime with low losses. By varying the capacitance in these metamaterials, a trade-off can be found between the operating frequency range and the magnitude of the effective nonlinearity, with potential enhancements of over one and two orders of magnitude in SHG and SPM, respectively. Due to the low losses, even higher efficiencies are supported in these structures, though with a less dramatic reduction in device length than the ELC and SRR mediums. Furthermore, the structures presented here were not optimized, and improved figures of merit should be achievable by varying the geometries and materials [50].

The SHG and SPM simulations and retrievals performed here are intended to be indicative of second-order and third-order nonlinear processes in general. That is to say, similar enhancements can be expected in the material figures of merit of any three-wave mixing and four-wave mixing processes, including those involving mixed polarizations, with the magnitudes depending on the amount of field localization and the mode overlap of the various interacting waves. However, it should be noted that deviation of one or more of the interacting frequencies from the resonant frequency will tend to reduce the overall enhancement in the resonant structures.

While the nonlinear dielectrics employed in these simulations were not modeled after any particular known substance, there are an abundance of materials that could be envisioned in this role. These include ferroelectrics, semiconductors, and the various glasses and polymers possessing relatively large nonlinearities [51,52]. Alternatively, the nonlinearities of metals themselves have been shown to be significant [53–57]. For certain structures, it may be that the nonlinearities of the metal are comparable to or even larger than the nonlinearities of the embedding medium. For metamaterials composed of nonlinear metallic nanostructures, the same principles and techniques employed here can be used to calculate the effective bulk nonlinearities, using an appropriate model for the local nonlinear processes in the metal components [58].

For fabrication concerns, no transverse feature sizes smaller than 100 nm were considered, and as such, these structures should be realizable by current techniques. In fact, for more accurate fabrication methods, these structures can be scaled to smaller dimensions and thus moved to higher operative frequencies while maintaining similar enhancement properties. However, for frequencies approaching the plasma frequency of silver, the effective losses will tend to increase, lowering the quality factors of the resonant structures [50]. The broadband structures, in contrast, should scale better, owing both to their simplified design and nonresonant nature.

In conclusion, we have demonstrated here, through full-wave simulations and by employing the transfer-matrix-based nonlinear retrieval method, a quantitative analysis of the enhancement of the effective nonlinearities of metamaterials

composed of periodic metallic structures embedded in nonlinear dielectrics. Our results confirm the prediction that nonlinear metamaterials can support drastically enhanced nonlinearities compared to their constituent elements, with improvements as high as two and four orders of magnitude for the second- and third-order material figures of merit, respectively. Such giant enhancements, together with the unique and configurable properties of metamaterials, have the potential to comprise the basis of a new generation of efficient and compact nonlinear devices.

ACKNOWLEDGMENTS

This work was supported by the Air Force Office of Scientific Research (Contract No. FA9550-09-1-0562). We thank Daniel J. Gauthier and Ekaterina Poutrina for helpful discussions.

APPENDIX: SECOND-HARMONIC GENERATION IN A DOUBLY NONLINEAR MEDIUM

We present here a derivation of the second-harmonic intensity in a medium with second-order nonlinear dependencies on the incident fields in both the electric polarization and magnetization. This analysis assumes plane waves with a single polarization, no losses, and real material parameters but can be extended to these more complex regimes by standard perturbations [59]. A similar development can be employed for other three- and four-wave mixing processes in a doubly nonlinear medium.

Let us consider a linearly polarized plane wave traveling with angular frequency ω through a homogeneous, isotropic medium. We orient our axes such that the electric field is along the x axis, magnetic field is along the y axis, and propagation is in the positive z direction. Using the convention that $Z_2 = \sqrt{\mu_2/\epsilon_2}$ and likewise for the other field variables, the x component of the second-order electric polarization at frequency 2ω is given by [33]

$$P^{(2)}(2\omega) = \tfrac{1}{2}\epsilon_0 \chi_e^{(2)}(2\omega;\omega,\omega)\,[E(\omega)]^2\,, \tag{A1}$$

where, owing to the linear polarization of the involved fields, we have substituted scalars for the usual vectors and tensors. The magnetization is defined in an analogous way:

$$M^{(2)}(2\omega) = \tfrac{1}{2}\chi_m^{(2)}(2\omega;\omega,\omega)\,[H(\omega)]^2\,. \tag{A2}$$

Thus, the material equations can be written as

$$D(2\omega) = \epsilon(2\omega)E(2\omega) + P^{(2)}(2\omega), \tag{A3}$$

$$B(2\omega) = \mu(2\omega)H(2\omega) + \mu_0 M^{(2)}(2\omega), \tag{A4}$$

where $\epsilon(\omega)$ and $\mu(\omega)$ are the absolute, frequency-dependent permittivity and permeability, respectively. For brevity, the frequency dependence of the field quantities will be denoted through subscripts.

We start from Maxwell's equations for time-harmonic fields, considering a second-order polarization *and* magnetization,

$$\vec{\nabla}\times\vec{H}_2 = -i2\omega(\epsilon_2\vec{E}_2 + \vec{P}^{(2)}), \tag{A5}$$

$$\vec{\nabla}\times\vec{E}_2 = i2\omega(\mu_2\vec{H}_2 + \mu_0\vec{M}^{(2)}), \tag{A6}$$

$$\vec{\nabla}\cdot\vec{D}_2 = 0, \tag{A7}$$

$$\vec{\nabla}\cdot\vec{B}_2 = 0. \tag{A8}$$

In the absence of the nonlinear terms and with the above assumptions, Eqs. (A5)–(A8) have solutions of the form

$$\vec{E}_2 = [e_2^+\exp(ik_2z) + e_2^-\exp(-ik_2z)]\hat{x}, \tag{A9}$$

$$\vec{H}_2 = [h_2^+\exp(ik_2z) + h_2^-\exp(-ik_2z)]\hat{y}, \tag{A10}$$

where $k_2 = 2\omega\sqrt{\epsilon_2\mu_2}$. We take the ansatz that the solutions in the presence of the nonlinearities are simply a perturbation of the solutions to the linear problem, where $e_2^{\pm}$ and $h_2^{\pm}$ are taken to be spatially varying in z. Furthermore, we assume the slowly varying amplitude approximation, such that the forward- and backward-propagating terms can be considered decoupled from each other and thus solved independently. Focusing solely on the forward propagating terms, we substitute our trial solutions into Eqs. (A5) and (A6), giving

$$-ik_2H_2 - \frac{dh_2}{dz}\exp(ik_2z) = -i2\omega(\epsilon_2E_2 + P^{(2)}), \tag{A11}$$

$$ik_2E_2 + \frac{de_2}{dz}\exp(ik_2z) = i2\omega(\mu_2H_2 + \mu_0M^{(2)}). \tag{A12}$$

We solve Eq. (A11) for H_2 and substitute this into Eq. (A12),

$$ik_2E_2 + \frac{de_2}{dz}\exp(ik_2z) = i2\omega\left\{Z_2\left[\epsilon_2E_2 + P^{(2)} + \frac{i}{2\omega}\frac{dh_2}{dz}\exp(ik_2z)\right] + \mu_0M^{(2)}\right\}, \tag{A13}$$

where $Z_2 = \sqrt{\mu_2/\epsilon_2}$ is the impedance of the medium. Rearranging and canceling terms, we arrive at the following expression:

$$\left(\frac{de_2}{dz} + Z_2\frac{dh_2}{dz}\right)\exp(ik_2z) = i2\omega(Z_2P^{(2)} + \mu_0M^{(2)}). \tag{A14}$$

Next, we introduce the quantity $\gamma = e_2 + Z_2h_2$ and use Eqs. (A1) and (A2) to give

$$\frac{d\gamma}{dz} = i\omega\left(Z_2\epsilon_0\chi_e^{(2)}e_1^2 + \mu_0\chi_m^{(2)}h_1^2\right)\exp(i\Delta kz), \tag{A15}$$

where $\Delta k = 2k_1 - k_2$ is the phase mismatch.

For simplicity, we assume the nondepleted pump approximation, such that e_1 and h_1 are constants that satisfy the linear form of Maxwell's equations with $e_1 = Z_1h_1$. Thus, the above equation can be integrated over an interaction length L with the boundary condition $\gamma(0) = 0$, giving

$$\gamma(L) = i\omega\sqrt{Z_2}\frac{e_1^2}{Z_1}\frac{\exp(i\Delta kL) - 1}{i\Delta k} \times\left(\epsilon_0Z_1\sqrt{Z_2}\chi_e^{(2)} + \mu_0\frac{1}{Z_1\sqrt{Z_2}}\chi_m^{(2)}\right). \tag{A16}$$

If at the point $z = L$ a significant amount of second-harmonic field has built up, we can take the approximation that $|\frac{de_2}{dz}(L)|$ and $|\mu_0\omega\chi_m^{(2)}h_1^2|$ are small compared to the other terms in Eq. (A12), implying that $ik_2E_2(L) = i2\omega\mu_2H_2(L)$, or

equivalently $e_2(L) = Z_2 h_2(L)$. Thus, in this limit, $\gamma(L) = 2e_2(L)$, and we find that

$$e_2(L) = i\frac{\omega}{2c}\frac{\sqrt{Z_2}}{Z_1}e_1^2\kappa^{(2)}\frac{\exp(i\Delta kL)-1}{i\Delta k}, \qquad \text{(A17)}$$

where we have introduced the material figure of merit

$$\kappa^{(2)} = \frac{Z_1\sqrt{Z_2}}{Z_0}\chi_e^{(2)} + \frac{Z_0}{Z_1\sqrt{Z_2}}\chi_m^{(2)} \qquad \text{(A18)}$$

and Z_0 is the impedance of free space. Looking at this equation, it is clear that the electric field at the second-harmonic is a phase-sensitive superposition of the contributions from the electric and magnetic nonlinearities alone. Subsequently, we define the fundamental and second-harmonic intensities according to

$$I_1 = \frac{1}{2Z_1}|e_1|^2, \qquad I_2(L) = \frac{1}{2Z_2}|e_2(L)|^2, \qquad \text{(A19)}$$

and finally obtain

$$I_2(L) = \frac{1}{2}\frac{\omega^2}{c^2}|\kappa^{(2)}|^2 I_1^2 L^2 \frac{\sin^2\left(\frac{\Delta kL}{2}\right)}{\left(\frac{\Delta kL}{2}\right)^2}. \qquad \text{(A20)}$$

[1] J. B. Pendry, D. Schurig, and D. R. Smith, Science **312**, 1780 (2006).
[2] D. R. Smith, W. J. Padilla, D. C. Vier, S. C. Nemat-Nasser, and S. Schultz, Phys. Rev. Lett. **84**, 4184 (2000).
[3] R. A. Shelby, D. R. Smith, and S. Schultz, Science **292**, 77 (2001).
[4] D. Schurig, J. J. Mock, B. J. Justice, S. A. Cummer, J. B. Pendry, A. F. Starr, and D. R. Smith, Science **314**, 977 (2006).
[5] J. B. Pendry, A. J. Holden, D. J. Robbins, and W. J. Stewart, IEEE Trans. Microwave Theory **47**, 2075 (1999).
[6] A. A. Zharov, I. V. Shadrivov, and Y. S. Kivshar, Phys. Rev. Lett. **91**, 037401 (2003).
[7] M. W. Klein, C. Enkrich, M. Wegener, and S. Linden, Science **313**, 502 (2006).
[8] I. V. Shadrivov, A. B. Kozyrev, D. W. van der Weide, and Y. S. Kivshar, Appl. Phys. Lett. **93**, 161903 (2008).
[9] F. Niesler, N. Feth, S. Linden, J. Niegemann, J. Gieseler, K. Busch, and M. Wegener, Opt. Lett. **34**, 1997 (2009).
[10] D. Huang, A. Rose, E. Poutrina, S. Larouche, and D. R. Smith, Appl. Phys. Lett. **98**, 204102 (2011).
[11] A. Popov and V. Shalaev, Appl. Phys. B **84**, 131 (2006).
[12] E. Poutrina, S. Larouche, and D. R. Smith, Opt. Commun. **283**, 1640 (2010).
[13] D. A. Powell, I. V. Shadrivov, Y. S. Kivshar, and M. V. Gorkunov, Appl. Phys. Lett. **91**, 144107 (2007).
[14] I. V. Shadrivov, A. B. Kozyrev, D. W. van der Weide, and Y. S. Kivshar, Opt. Express **16**, 20266 (2008).
[15] B. Wang, J. Zhou, T. Koschny, and C. M. Soukoulis, Opt. Express **16**, 16058 (2008).
[16] D. Huang, E. Poutrina, and D. R. Smith, Appl. Phys. Lett. **96**, 104104 (2010).
[17] A. Rose, D. Huang, and D. R. Smith, Phys. Rev. Lett. **107**, 063902 (2011).
[18] E. Poutrina, D. Huang, and D. R. Smith, New J. Phys. **12**, 093010 (2010).
[19] S. Larouche and D. R. Smith, Opt. Commun. **283**, 1621 (2010).
[20] A. Rose, S. Larouche, D. Huang, E. Poutrina, and D. R. Smith, Phys. Rev. E **82**, 036608 (2010).
[21] K. B. Crozier, A. Sundaramurthy, G. S. Kino, and C. F. Quate, J. Appl. Phys. **94**, 4632 (2003).
[22] P. Mhlschlegel, H.-J. Eisler, O. J. F. Martin, B. Hecht, and D. W. Pohl, Science **308**, 1607 (2005).
[23] E. C. Le Ru, E. Blackie, M. Meyer, and P. G. Etchegoin, J. Phys. Chem. C **111**, 13794 (2007).
[24] S. Kim, J. Jin, Y.-J. Kim, I.-Y. Park, Y. Kim, and S.-W. Kim, Nature (London) **453**, 757 (2008).
[25] J. A. Schuller, E. S. Barnard, W. Cai, Y. C. Jun, J. S. White, and M. L. Brongersma, Nat. Mater. **9**, 193 (2010).
[26] M. Soljacic and J. D. Joannopoulos, Nat. Mater. **3**, 211 (2004).
[27] J. Bravo-Abad, A. Rodriguez, P. Bermel, S. G. Johnson, J. D. Joannopoulos, and M. Soljacic, Opt. Express **15**, 16161 (2007).
[28] A. Ashkin, G. Boyd, and J. Dziedzic, IEEE J. Quantum Electron. **2**, 109 (1966).
[29] V. Berger, J. Opt. Soc. Am. B **14**, 1351 (1997).
[30] S. Larouche, A. Rose, E. Poutrina, D. Huang, and D. R. Smith, Appl. Phys. Lett. **97**, 011109 (2010).
[31] D. S. Bethune, J. Opt. Soc. Am. B **6**, 910 (1989).
[32] D. R. Smith, Phys. Rev. E **81**, 036605 (2010).
[33] R. W. Boyd, *Nonlinear Optics* (Academic, Burlington, MA, USA, 2008).
[34] C. R. Simovski, Metamaterials **1**, 62 (2007).
[35] C. R. Simovski and S. A. Tretyakov, Phys. Rev. B **75**, 195111 (2007).
[36] C. Simovski, Opt. Spectrosc. **107**, 726 (2009).
[37] COMSOL [http://www.comsol.com].
[38] P. B. Johnson and R. W. Christy, Phys. Rev. B **6**, 4370 (1972).
[39] D. R. Smith, S. Schultz, P. Markoš, and C. M. Soukoulis, Phys. Rev. B **65**, 195104 (2002).
[40] X. Chen, T. M. Grzegorczyk, B.-I. Wu, J. Pacheco, and J. A. Kong, Phys. Rev. E **70**, 016608 (2004).
[41] D. R. Smith, D. C. Vier, T. Koschny, and C. M. Soukoulis, Phys. Rev. E **71**, 036617 (2005).
[42] *Nonlinear Optical Effects and Materials*, edited by P. Günter (Springer, Berlin, Germany, 2000).
[43] D. Schurig, J. J. Mock, and D. R. Smith, App. Phys. Lett. **88**, 041109 (2006).
[44] S. Larouche, A. Rose, and D. R. Smith (to be submitted, 2011).
[45] T. Koschny, P. Markoš, D. R. Smith, and C. M. Soukoulis, Phys. Rev. E **68**, 065602 (2003).
[46] I. V. Shadrivov, A. A. Zharov, and Y. S. Kivshar, J. Opt. Soc. Am. B **23**, 529 (2006).
[47] A. Rose and D. R. Smith, Phys. Rev. A **84**, 013823 (2011).
[48] A. Rose and D. R. Smith Opt. Mater. Express **1**, 1232 (2011).

[49] S. O'Brien, D. McPeake, S. A. Ramakrishna, and J. B. Pendry, Phys. Rev. B **69**, 241101 (2004).
[50] D. O. Güney, T. Koschny, and C. M. Soukoulis, Phys. Rev. B **80**, 125129 (2009).
[51] *Molecular Nonlinear Optics: Materials, Physics and Devices*, edited by J. Zyss (Academic, San Diego, 1994).
[52] V. G. Dmitriev, G. G. Gurzadyan, and D. N. Nikogosyan, Handbook of Nonlinear Optical Crystals (Springer, Berlin, Germany, 1997).
[53] A. Nahata, R. A. Linke, T. Ishi, and K. Ohashi, Opt. Lett. **28**, 423 (2003).
[54] D. Krause, C. W. Teplin, and C. T. Rogers, J. Appl. Phys. **96**, 3626 (2004).
[55] N. I. Zheludev and V. I. Emel'yanov, J. Opt. A **6**, 26 (2004).
[56] M. W. Klein, M. Wegener, N. Feth, and S. Linden, Opt. Express **15**, 5238 (2007).
[57] D. T. Owens, C. Fuentes-Hernandez, J. M. Hales, J. W. Perry, and B. Kippelen, J. Appl. Phys. **107**, 123114 (2010).
[58] M. Scalora, M. A. Vincenti, D. de Ceglia, V. Roppo, M. Centini, N. Akozbek, and M. J. Bloemer, Phys. Rev. A **82**, 043828 (2010).
[59] A. Yariv, *Quantum Electronics* (Wiley, New York, 1989).